Enhanced spin wave propagation in magnonic rings by bias field modulation

G. Venkat,[1,a] D. Venkateswarlu,[2] R. S. Joshi,[2] M. Franchin,[3] H. Fangohr,[3,4] P. S. Anil Kumar,[2] and A. Prabhakar[1]
[1]*Department of Electrical Engineering, Indian Institute of Technology Madras, Chennai 600036, India*
[2]*Department of Physics, Indian Institute of Science, Bangalore 560012, India*
[3]*Engineering and the Environment, University of Southampton, Southampton SO17 1BJ, United Kingdom*
[4]*European XFEL GmbH, Holzkoppel 4, 22869 Schenefeld, Germany*

(Presented 7 November 2017; received 26 September 2017; accepted 18 October 2017; published online 8 December 2017)

We simulate the spin wave (SW) dynamics in ring structures and obtain the $\omega - k$ dispersion relations corresponding to the output waveguide. Different bias field configurations affect the transfer of SW power from one arm of the structure to the other arm. To this end, we show that circular or radial bias fields are more suitable for energy transfer across the ring than the conventional horizontal bias field $\mathbf{H}_x$. The SW dispersion shows that modes excited, when the bias field is along the ring radius, are almost 10 dB higher in power when compared to the modal power in the case of $\mathbf{H}_x$. This is also corroborated by the SW energy density in the receiving stub.
https://doi.org/10.1063/1.5006576

I. INTRODUCTION

Magnetic nano structures can be designed into functional devices.[1] They are being studied in a variety of shapes and materials for both fundamental studies and engineering applications.[2] In particular ferromagnetic nano rings have received some attention due to their geometry related advantages.[3–5] They are being used to study domain wall nucleation and motion.[6,7] These ring structures also offer the advantage of helping us understand the effects of the interference of spin waves (SWs).[8] In recent times, they have been used to obtain the dynamic susceptibility of onion states and probe spin waves modes in out of plane configurations.[9]

Computational micromagnetics, where the Landau-Lifshitz (LL) equation is solved numerically is suitable for studying SW dynamics of ferromagnetic structures.[10] Experimental studies typically extract the field dispersion relations $\omega(H)$.[11,12] The dispersion can also be probed over a partial range of the Brillouin zone using Brillouin light spectroscopy.[13]

However, using simulations, we can obtain a more detailed picture of the $\omega - k$ relation for spin waves.[14] Magnetization studies of ring nanostructures are available for the finite difference (FD) micromagnetic simulations with OOMMF[15] as the solver.[16–18] Here we use the FD simulator Mumax3[19] which allows us to run simulations using GPUs (graphical processing units) and get considerable gains in simulation running times. Since the geometry is not rectangular, we have also validated our simulations with the finite element (FE) method solver Nmag.[20,21]

We investigate the SW dynamics in a ring with two stubs and study the effects of varying the external bias fields on the amplitude and energy of the SWs transferred to the Rx stub. We find that there is an increase in transferred SW energy for radial and circular bias fields when compared to the

[a]Electronic mail: guruvenkat7@gmail.com

more conventional case of a horizontal bias field. We study the reasons for this increase in energy and summarize our observations.

II. GEOMETRY AND SIMULATION METHODOLOGY

A ring structure with an attached stub on either side, as shown in Fig. 1, is considered. The ring is made of permalloy ($Ni_{80}Fe_{20}$), which is commonly used to study spin waves. The material parameters[22] used in the simulations are the saturation magnetization $M_s = 8.6 \times 10^5$ A/m, exchange constant $A = 13 \times 10^{-12}$ J/m, anisotropy constant $K = 0$ and gyromagnetic ratio $\gamma = 175.866$ GHz/T.

The structure was designed to excite SWs in the left stub (Tx), allow them to propagate along the arms of the ring and then receive them in the right stub (Rx). Absorbing boundary layers were introduced in both the Tx and Rx stubs so that reflections from the structure edges do not affect our estimates of energy transfers. We assume a parabolic variation of the LL damping constant α in the ABL, which was found to be sufficient to curb SW reflections from the edges of the geometry.[23] Different bias configurations affects the amount of SW energy reaching the Rx stub. We choose a thickness of 5 nm and focus on the effect of bias field variations in the plane of the ring.

The average length of an edge element plays an important role in micromagnetic simulations. Since the exchange length for permalloy is ~ 5.7 nm, and we used a cell size of 5 nm for the Mumax3 simulations, we were able to resolve the exchange dominated SWs. For Nmag simulations, we used a mesh generated by the package Gmsh.[24] The mesh had 160268 volume elements, 96468 surface elements and an average edge length of 5.12 nm.

A. Simulation methodology

The simulation methodology is similar to what is explained in our proposal for a standard spin wave problem.[14] The structure was initially brought to a saturated ground state by applying a high enough bias, with $H_0 = 10.1$ kOe, for different bias field directions. This ground state was saved and given as initial magnetization to the second stage of the simulation where both the bias $\mathbf{H}_0$ and the excitation $\mathbf{h}(t)$ were applied.

We aim for the magnetic excitation pulse to excite spin waves of reasonable amplitude uniformly over a sufficiently large frequency range. The pulse was applied uniformly (in space) over the stub area (of area 100×100 nm^2), of the left stub, shown in Fig. 1. In time, it varies as a sinc pulse,

$$|\mathbf{h}|(t) = \Gamma \frac{\sin(\omega_c (t - t_0))}{\omega_c (t - t_0)}, \tag{1}$$

where the cutoff frequency $f_c = \omega_c/(2\pi) = 200$ GHz, $t_0 = 50$ ps and the amplitude $\Gamma = 5$ kOe.

We then save the discrete magnetization as a function of space and time, namely $\mathbf{m}(x_i, y_j, z_k, t_n)$. To extract the SW dispersion, we keep two variables, y and z, constant and obtain $\mathbf{m}(x_i, t_n)$. The component of $\mathbf{m}$ along the excitation, $m_y(x_i, t_n)$, is considered and its 2-D Fourier transform $\tilde{m}_y(k_{x_i}, f_n)$ is calculated. The dispersion relations are visible on a surface plot of $10 \log_{10}\left(|\tilde{m}_y(k_{x_i}, f_n)|^2\right)$ as

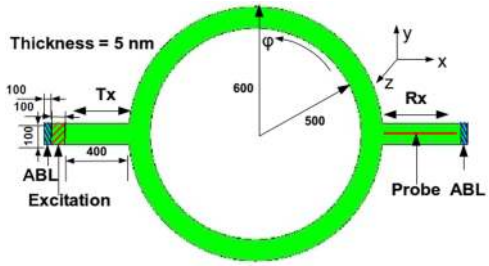

FIG. 1. The geometry of the ring structure. The region with red stripes in the Tx stub is the area over which the excitation is uniformly applied. The dispersion is probed along the central red line in the Rx stub. The region with blue stripes at the end of both the Tx and Rx stubs are the absorbing boundary layers. The dimensions are all in nm.

parabolas. By applying a Hanning window to $m_y(x_i, t_n)$, before taking the Fourier transform, we reduce spectral leakage and scalloping loss.[25] We also apply a third-order Savitzky-Golay filter with 51 taps to smoothen the dispersion curves and remove numerical artifacts from them.[26] The order and number of taps of the filter were obtained after due optimization.

III. THE SIMULATION CONFIGURATIONS

Different bias field configurations, shown in Fig. 2, allow for backward volume (BV), and surface SWs to propagate in the structure. The curved bias fields followed the stable "onion" and "vortex" magnetization states in the ring. In some cases, a combination of these different types of SWs will propagate, affecting the energy transfer between Tx and Rx stubs.

A. Simulation 1: The uniform state

The bias was of the form

$$\mathbf{H}_x = H_0\hat{x}. \tag{2}$$

The bias configuration and type of SW propagation is shown in Fig. 2. A majority of the moments are oriented along the x axis, although there will be minor deviations caused by the shape anisotropy of the ring. On excitation, BV SWs propagate into the Tx stub. But, the energy must then be split between surface and BV waves in the left half of the ring, convert to BV type at the top and bottom of the ring, again get transformed to a combination of BV and surface in the right half of the ring and finally end up as BV type in the Rx stub (Fig. 2). We expected this to be a potentially degrading process as multiple interferences between different wave configurations could affect energy transfer from Tx to Rx.

B. Simulation 2: The onion state

The bias was of the form

$$\mathbf{H}_{\mathrm{ON}} = \begin{cases} H_0\hat{x} & \text{in the Tx and Rx stubs} \\ -H_0\hat{\phi} & \text{in the upper half of the ring} \\ H_0\hat{\phi} & \text{in the lower half of the ring} \end{cases}. \tag{3}$$

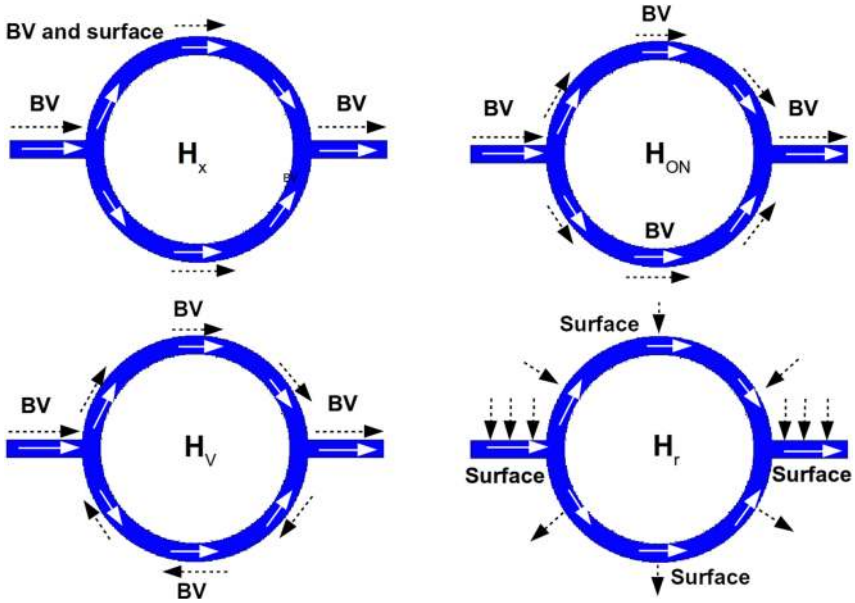

FIG. 2. Different types of SWs propagating in the structure for the uniform, onion, vortex and radial ground states. The black arrows represent the direction of $\mathbf{H}_0$ while the white arrows represent the direction of SW propagation. The regions of propagation of backward volume (BV) and surface waves are appropriately marked.

Here $\hat{\phi}$ is the unit vector tangential to the ring and positive in the anticlockwise direction. We respect the conditions imposed by the shape anisotropy of the curved surface, and always apply the bias field parallel to the edge of the structure, thus preferentially supporting BV waves. Since the BV SW configuration is maintained, we expect to see better energy transfer between the Tx and Rx stubs.

C. Simulation 3: The vortex state

Similar to the onion state, the vortex state also has a bias parallel to the edges of the geometry. But, in contrast with the onion state, the bias field is now axially symmetric. With

$$\mathbf{H}_{\mathrm{V}} = \begin{cases} H_0\hat{x} & \text{in the Tx and Rx stubs} \\ -H_0\hat{\phi} & \text{in the ring} \end{cases}, \tag{4}$$

we again have BV waves flowing around the ring. Such a bias field may be designed into an experiment using a current carrying conductor passing through the centre of the ring.

D. Simulation 4: Radial bias field

We also consider a bias field generated by a current carrying ring present under the magnonic ring. This bias field is a modification of what is experimentally used in studying how spin turn at a corner,[27] using a copper split ring as the under layer. With the current being injected from Tx to Rx, the bias field will be

$$\mathbf{H_r} = \begin{cases} -H_0\hat{y} & \text{in the Tx and Rx stubs} \\ -H_0\hat{r} & \text{in the top half of the ring} \\ H_0\hat{r} & \text{in the bottom half of the ring} \end{cases}, \tag{5}$$

and is shown in Fig. 2. Here $\hat{r}$ is the unit vector in the outward radial direction. With this bias field, we sustain surface waves throughout the structure and we again expect increased transfer of SW energy from Tx to Rx. In this case the excitation field, given in (1), is applied along **x**.

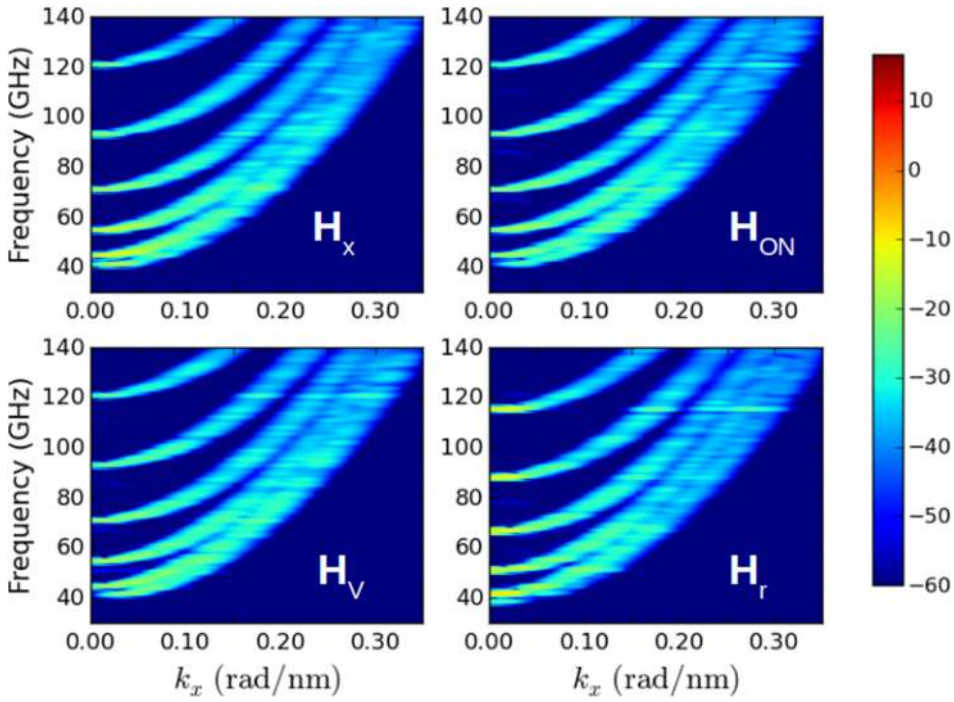

FIG. 3. Surface plots of the SW power spectrum for the different bias fields. The colorbar corresponds to the SW power in a dB scale. The multiple modes correspond to the quantization along the width of the Rx stub.

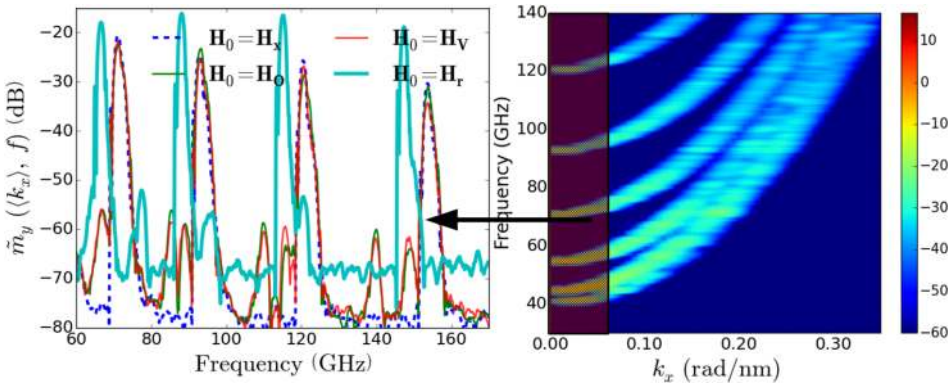

FIG. 4. The Fourier power averaged over $k_x = 0$ to 0.05 rad/nm. The modes formed with $\mathbf{H}_r$ are of higher power than when $\mathbf{H}_0 = \mathbf{H}_x$.

IV. SIMULATION RESULTS AND DISCUSSIONS

Fig. 3 shows the dispersion curve along the central line (at $y = 0$ and $z = 0$) in Rx, which is shown in Fig. 1, for the different bias fields. Since the spin waves are exchange dominated, the dispersion relations exhibit forward volume characteristics $\left(\frac{\partial \omega}{\partial k} > 0\right)$ even though only BV and surface wave configurations exist in the simulations.[14] The frequency of the fundamental mode (40 GHz) corresponds to a maximum of the dipole dominated BV spin wave manifold. The different modes arise due to the finite width of the stub and correspond to the different quantizations along the width. With the spatially uniform excitation, given by (1), we preferentially excite the symmetric width modes.

We obtain the Fourier power along f and average it over $k_x = 0$ to 0.05 rad/nm, for the different bias fields. This range of k_x corresponds to longer wavelength SWs and are easier to excite in an experiment. These averaged power scans are shown in Fig. 4. The modal powers for the curved bias fields which involve the propagation of backward volume SWs are almost the same. SW modes in the case of $\mathbf{H}_r$ are at different frequencies due to having different dispersion relations.[14] These surface modes show almost 10 dB higher power than the other bias fields. This indicates that having the bias normal to the ring leads to more adiabatic transfer of energy into the Rx stub. We understand this further by looking at the energy of the SWs in the Tx stub.

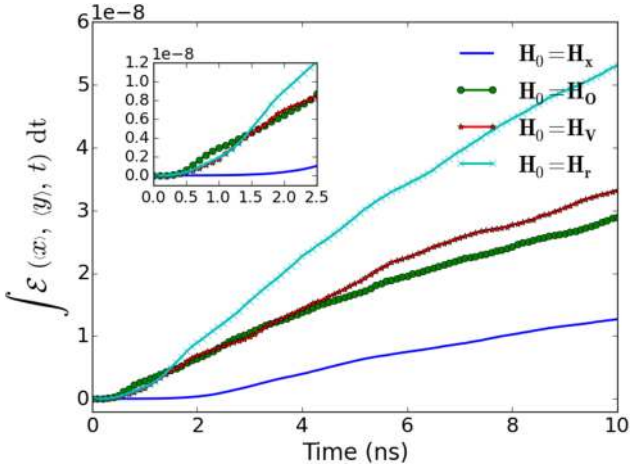

FIG. 5. The cumulative energy density as a function of time in the Rx stub for different bias fields. The $\mathbf{H}_{ON}$, $\mathbf{H}_V$ and $\mathbf{H}_r$ fields show a higher energy build up when compared to $\mathbf{H}_x$.

A. SW energy density

The energy density of these spin waves are given by

$$\mathcal{E}(x,\ y,\ t) = -\frac{1}{2}\mathbf{M}(x,\ y,\ t).\mathbf{B}(x,\ y,\ t), \tag{6}$$

where $\mathbf{B}$ is the instantaneous magnetic flux density and $\mathbf{M}$ is the magnetization. The cumulative energy density for the different bias fields are shown in Fig. 5. Note that the static energy density i.e. $\mathcal{E}(x,\ y,\ t=0)$ has been deducted in each case. Since we have considered a lossless case here ($\alpha = 0$), the energy in Rx stub keeps increasing. We observe that $\mathbf{H}_{\mathrm{ON}}$ and $\mathbf{H}_{\mathrm{V}}$ show a threefold increase and $\mathbf{H}_r$ shows the maximum energy transfer with a five fold increase when compared to that of $\mathbf{H}_x$.

The inset plot in Fig. 5 shows that $\mathbf{H}_{\mathrm{ON}}$, $\mathbf{H}_{\mathrm{V}}$ and $\mathbf{H}_r$ also lead to faster SW transfer with SWs starting to enter Rx at 500 ps while it takes about 2ns for $\mathbf{H}_x$. This increase in SW group velocity is due to preserving the SW configuration throughout the structure.

V. SUMMARY

We have studied SW dynamics in ring structures and have increased SW coupling efficiency between the Tx and Rx stubs by changing the bias field configurations. The results presented here have been obtained by running FDTD simulations using Mumax3 which have the advantage of larger computational speeds. We obtain the dispersion of SWs in the Rx stub and show that the SW modes have almost 10 dB higher power when the bias fields are radial. The SW energy density in Rx show at least three fold increase when circular or radial bias fields are applied. These bias fields also lead to an increase in SW group velocity due to preserving the SW configuration throughout the structure.

ACKNOWLEDGMENTS

This research has received funding from the European Community's Seventh Framework Programme (FP7/2007-2013) and from the DST, Government of India under the India-EU collaborative project DYNAMAG (grant number INT/EC/CMS (24/233552)).

[1] D. Sander *et al.*, "The 2017 magnetism roadmap," Journal of Physics D: Applied Physics **50**, 363001 (2017).
[2] V. V. Kruglyak *et al.*, "Magnonics," J. Phys. D: App. Phys. **3**, 264001 (2010).
[3] M. Y. Rafique *et al.*, "Switching behavior and novel stable states of magnetic hexagonal nanorings," J. Magn. Magn. Mater. **432**, 1 (2017).
[4] M. Lal *et al.*, "Control of stable magnetization states in permalloy nanorings using magnetic nanowires," J. Magn. Magn. Mater. (2017).
[5] X. Zhou *et al.*, "Spin wave modes in out-of-plane magnetized nanorings," Phys. Rev. B **96**, 024446 (2017).
[6] K. Richter *et al.*, "Localized domain wall nucleation dynamics in asymmetric ferromagnetic rings revealed by direct time-resolved magnetic imaging," Phys. Rev. B **94**, 024435 (2016).
[7] M. A. Mawass *et al.*, "Switching by domain-wall automotion in asymmetric ferromagnetic rings," Phys. Rev. Applied **7**, 044009 (2017).
[8] J. Podbielski *et al.*, "Spin-wave interference in microscopic rings," Phys. Rev. Lett. **96**, 167207 (2006).
[9] X. Zhou *et al.*, "Spin wave modes in out-of-plane magnetized nanorings," Physical Review B **96**, 024446 (2017).
[10] V. Kruglyak and R. Hicken, "Magnonics: Experiment to prove the concept," J. Magn. Magn. Mater. **306**, 191 (2006).
[11] F. Giesen *et al.*, "Multiple ferromagnetic resonance in mesoscopic permalloy rings," J. Appl. Phys. **97**, 10A712 (2005).
[12] G. Gubbiotti *et al.*, "Splitting of spin excitations in nanometric rings induced by a magnetic field," Phys. Rev. Lett. **97**, 247203 (2006).
[13] S. Demokritov *et al.*, "Brillouin light scattering studies of confined spin waves: Linear and nonlinear confinement," Phys. Rep. **348**, 441 (2001).
[14] G. Venkat *et al.*, "Proposal for a standard micromagnetic problem: Spin wave dispersion in a magnonic waveguide," IEEE Trans. Magn. **49**, 524 (2013).
[15] M. Donahue and D. Porter, "OOMMF user's guide, version 1.0," tech. rep., National Institute of Standards and Technology, Gaithersburg, MD, 1999.
[16] G. D. Chaves-O'Flynn *et al.*, "Micromagnetic simulations of ferromagnetic rings," J. Appl. Phys **103**, 07D917 (2008).
[17] J. Wang *et al.*, "Micromagnetic calculation of dynamic susceptibility in ferromagnetic nanorings," J. Appl. Phys. **105**, 083908 (2009).
[18] J. Palma *et al.*, "Micromagnetic simulation of Fe asymmetric nanorings," J. Magn. Magn. Mater. **324**, 637 (2012).
[19] A. Vansteenkiste *et al.*, "The design and verification of MuMax3," AIP Advances **4**(10), 107133 (2014).

[20] H. Fangohr, M. Albert, and M. Franchin, "Nmag micromagnetic simulation tool: Software engineering lessons learned," in *Proceedings of the International Workshop on Software Engineering for Science, SE4Science '16*, (New York, NY, USA), p. 1, ACM, 2016.
[21] T. Fischbacher *et al.*, "A systematic approach to multiphysics extensions of finite-element-based micromagnetic simulations: Nmag," IEEE Trans. Magn. **43**, 2896 (2007).
[22] A. Hubert and R. Schafer, *Magnetic Domains: The Analysis of Magnetic Microstructures* (Springer, Berlin, 1998).
[23] G. Venkat and A. Prabhakar, "Absorbing boundary layers for spin wave micromagnetics," J. Magn. Magn. Mater. (2017).
[24] C. Geuzaine and J. Remacle, "Gmsh: A 3-D finite element mesh generator with built-in pre- and post-processing facilities," Int. J. Numer. Meth. Eng. **79**, 1309 (2009).
[25] D. Kumar *et al.*, "Numerical calculation of spin wave dispersions in magnetic nanostructures," J. Phys. D: Appl. Phys. **45**, 015001 (2012).
[26] A. Savitzky and M. J. E. Golay, "Smoothing and differentiation of data by simplified least squares procedures," Anal. Chem. **36**, 1627 (1964).
[27] K. Vogt *et al.*, "Spin waves turning a corner," Appl. Phys. Lett. **101**, 042410 (2012).